

RSC Advances



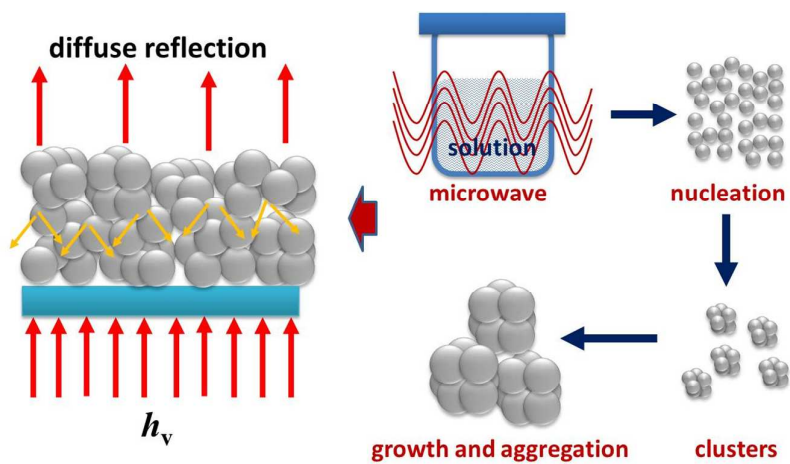
This is an *Accepted Manuscript*, which has been through the Royal Society of Chemistry peer review process and has been accepted for publication.

Accepted Manuscripts are published online shortly after acceptance, before technical editing, formatting and proof reading. Using this free service, authors can make their results available to the community, in citable form, before we publish the edited article. This *Accepted Manuscript* will be replaced by the edited, formatted and paginated article as soon as this is available.

You can find more information about *Accepted Manuscripts* in the [Information for Authors](#).

Please note that technical editing may introduce minor changes to the text and/or graphics, which may alter content. The journal's standard [Terms & Conditions](#) and the [Ethical guidelines](#) still apply. In no event shall the Royal Society of Chemistry be held responsible for any errors or omissions in this *Accepted Manuscript* or any consequences arising from the use of any information it contains.

Table of Contents



Hierarchically TiO₂ nanocrystallite aggregates are obtained by microwave synthesis in a few minutes that show high light scattering and larger surface area for improving the performance of dye-sensitized solar cells.

ARTICLE

Rapid constructing TiO₂ aggregates using microwave assisted synthesis and its application for dye-sensitized solar cells

Cite this: DOI: 10.1039/x0xx00000x

Received 00th January 2012,

Accepted 00th January 2012

DOI: 10.1039/x0xx00000x

www.rsc.org/

Xuyang Wang^a, Jianjun Tian^{a*}, Chengbin Fei^b, Lili Lv^a, Yajie Wang^b, Guozhong Cao^{b,c*}

Hierarchically TiO₂ nanocrystallite aggregates with size of ~500 nm consisted of ~10 nm nanocrystallites have been synthesized by microwave assisted method at 150 °C in a short time (~10 minutes) for the application as the photoanode of dye-sensitized solar cells (DSCs). Ethanol and TiCl₄ are selected as the solvent and titanium precursor, respectively. The rapid heating rate and superheating / “hot spots” of the reaction system under microwave irradiation result in huge amounts of nucleuses instantly so as to form great deal of clusters. The clusters grow up rapidly, meanwhile, are assembled to TiO₂ nanocrystallite aggregates. The TiO₂ aggregates show the better light scattering property, larger specific surface area and higher dye-loading than those of the commercial P25 TiO₂ nanoparticles. In comparison with P25, the short current density (J_{sc}) and dye-loading of DSC based the as-synthesized TiO₂ aggregates increase by 33% and 62%, respectively. At a result, the PCE of the DSC is up to 7.64%. The TiO₂ aggregates obtained by microwave assisted synthesis show a promising and potential candidate for DSCs.

1. Introduction,

Mesoporous oxide semiconductors (MOS) has been regarded as an attractive material for the solar cells, solar fuel, photo catalyst and energy storage devices due to their high surface area, excellent photoelectric and electrochemical properties^{1, 2}. Among various MOSs, anatase titanium dioxide (TiO₂) has been studied widely in the dye-sensitized solar cells (DSCs), which were first reported by Oregan and Grätzel at 1991³. Due to the low cost of the production, DSCs have become a cause for certain attention in the field of photovoltaic. The MOS TiO₂ film is one of the key components in such cells, which plays an important role in the adsorption of dyes and electronic transmission⁴⁻¹⁰. Recently, power conversion efficiency (PCE) in DSCs devices based on MOS TiO₂ film has achieved as high as 13% using a molecularly engineered porphyrin dye, coded SM315 under full sun illumination (AM 1.5G, 100 mW/cm²)¹¹.

A lot of research has been done on the synthesis of a variety of TiO₂ nanostructures in the forms of wires, tubes, spheres, rods, sheets, belts, flowers and trees for the efficient DSC devices¹²⁻¹⁶. To increase the electron mobility, one-dimensional (1D) TiO₂ nanostructures, such as nanotube arrays and single-crystalline nanowire arrays, have been studied as photoanodes for DSCs¹². However, DSCs based on 1D structures have not reached high conversion efficiency as expected due to the much small surface area for dye adsorption¹⁷. The 3D hierarchical nanostructures can offer larger surface areas for dye adsorption while simultaneously enhancing light scattering for efficient photon harvesting, and

thereby, improving power conversion efficiency¹⁶⁻¹⁹. The aggregate structure consisting of primary nanocrystallites can provide both large specific surface area and light scattering effect so as to enhance the performance of DSCs¹⁹⁻²⁵. The previous works showed that the photoanodes with the hierarchical aggregates structure are promising for the highly efficiency DSCs.

In the last few decades, many methods have been used to synthesize TiO₂ nanostructures, such as Sol-Gel²⁶, hydrothermal²⁷, solvothermal²⁸ and template²⁹ approaches. The hydrothermal and solvothermal methods have been frequently used for the reason that it is capable of obtaining the desired size and structure of TiO₂ nanocrystals by controlling the temperature, duration, concentration of the reaction. However, defects like complex and time-consuming process have been pointed out in the hydrothermal and solvothermal methods. The high cost and low productivity of the hydrothermal and solvothermal methods are considered as a big hindrance for their applications in DSCs. There is growing need to develop a fast and high productivity synthesis method to obtain TiO₂ nanocrystals for the application in DSCs. Compared with hydrothermal and solvothermal methods, the microwave assisted synthesis offers rapid processing speed, homogeneous heating and simple control of processing conditions, and thus has attracted much attention in the last few years³⁰. So the microwave assisted synthesized TiO₂ nanocrystallites have shown their potentials as photoanodes for DSCs in recent studies³¹⁻³⁵. For examples, Dar et al³¹ synthesized TiO₂ nanoparticles (~7 nm) and nanospheres (100-400 nm) of TiO₂ from the same precursor using a microwave assisted approach. After using these nanostructures as a photoanode in DSCs, a modest yet

appreciable efficiency of 6.5% was achieved. Manseki et al³² prepared the highly crystallized TiO₂ nanorods by the microwave assisted method to construct a photoanode for DSCs. Shen et al³⁵ reported the pure anatase TiO₂ nanoparticles with size about 20 nm were obtained by the microwave assisted method for DSCs. PCE of the solar cells based the nanoparticles was up to 7.7%. So the microwave assisted synthesis is considered as a facile, energy-saving and mass production scalable approach to replace the hydrothermal and solvothermal processes without sacrificing the photovoltaic performances of DSCs.

In this study, the microwave assisted synthesis has been taken to synthesize hierarchically TiO₂ nanocrystallite aggregates. Ethanol and TiCl₄ are selected as the solvent and titanium precursor, respectively. The nearly spherical TiO₂ aggregates with size of ~500 nm consisted of ~10 nm nanocrystallites, which show better light scattering property, larger specific surface area and higher dye-loading than those of the commercial P25 TiO₂ nanoparticles. In comparison with P25 TiO₂ photoanode, the short current density (J_{sc}) and dye-loading of the DSC based as-synthesized aggregates TiO₂ photoanode increase by 33% and 62%, respectively. At a result, the PCE of the DSC reaches 7.64%. The possible mechanisms for such enhancement in the power conversion efficiency have been discussed.

2. Results and discussion,

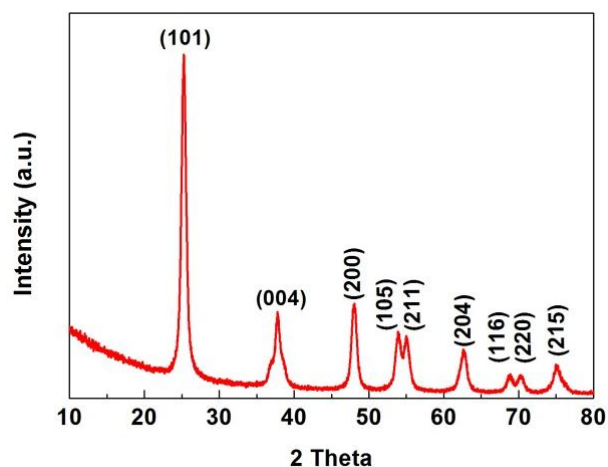


Figure 1. XRD pattern of the as-synthesized TiO₂ powder by microwave assisted method.

The TiO₂ nanocrystallites are prepared by microwave assisted synthesis at 150 °C for only 10 minutes in this paper. Figure 1 shows the XRD pattern of the as-synthesized dry solid powder by microwave assisted method. The XRD peaks can be indexed to the anatase structure of standard TiO₂ (JCPDS 21-1272). To within the detection limit of XRD, no peak characteristic of any impurity is found in the as-synthesized powder, indicating the as-synthesized product is a pure anatase TiO₂ phase. The SEM images of as-synthesized TiO₂ samples are presented in Figure 2 (a) and (b). The presence of the TiO₂ nanocrystallite aggregates assembled by agglomerated nanoparticles with sizes of ~10 nm was observed. The TiO₂ nanocrystallite aggregates possess a size of ~500 nm in diameter and show nearly spherical morphology. The mesoporous film prepared by TiO₂ aggregates can serve as organic dyes scaffold to collect and transfer the excited electrons from the dyes. This film has much more porous with voids as large as several micrometers, which facilitates dyes to permeate into the interior of the film. In

addition, the aggregates contain a huge amount of nanoparticles, which leads to the largeness of the specific surface to absorb much more dyes. Figure 2 (c) and (d) show the HRTEM images of the TiO₂ aggregates. It is can be seen that the nanocrystallite cluster is assembled by single crystals with size of ~5nm, corresponding to the anatase (101) facet (see FFT patterns). So the crystal growth is favorably along the [101] direction during microwave assisted synthesis process.

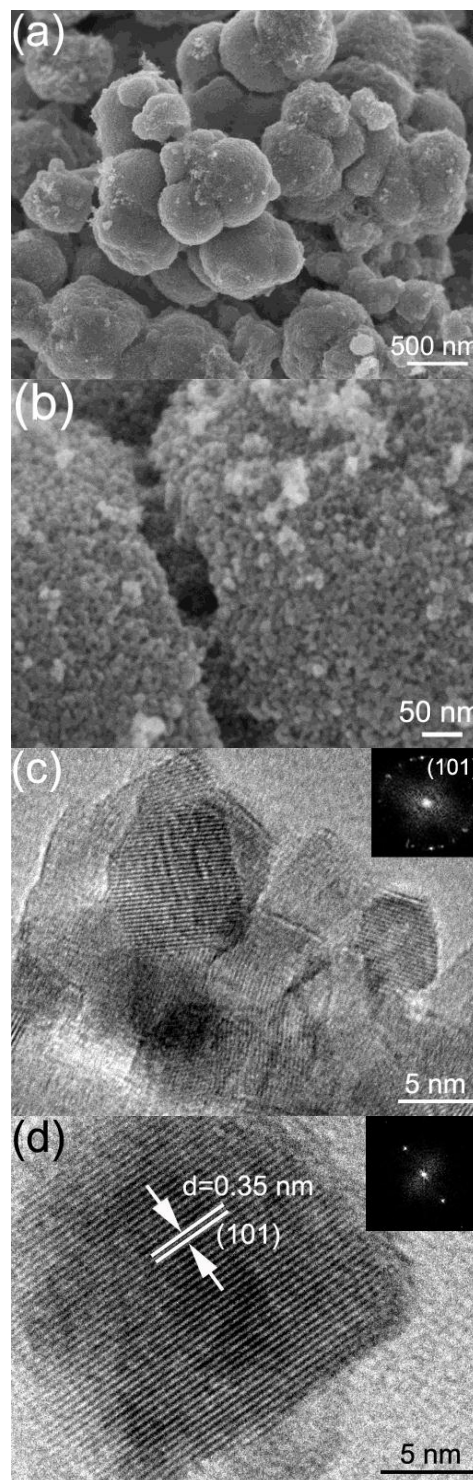


Figure 2. SEM images (a, b) and (c, d) HRTEM images of as-synthesized TiO₂ aggregates, inset showing the fast Fourier transform (FFT) diffraction pattern.

In this study, TiCl_4 and ethanol are selected as the titanium precursor and solvent, respectively. TiCl_4 is widely used for titania synthesis and is very reactive to water or oxygen, forming titanium hydroxide. It is to be noted that the reaction in the medium ethanol is very slow at room temperature. Reaction temperatures of 80~150 °C are generally required to obtain reasonable rates and crystalline products³⁶. Figure 3 (a) displays the La-Mer model for nucleation and growth kinetics of nanoparticles³⁷. The process of formation of nanocrystals is classically divided into two events: nucleation and growth. When the supersaturation is relieved by the formation of nuclei, the system enters the growth stage, in which no additional nuclei are formed but only existing clusters grow larger³⁶⁻³⁸. The nucleation and growth processes can be influenced by heating rate. As for microwave assisted synthesis, the mixture solution is heated to the reaction temperature (~150 °C) in a very short time (1-3 minutes), which leads to form a huge amount of crystal nucleus. Once the nucleation starts, the reaction system immediately enters the growth process and nucleus grow up rapidly. The overall processes containing nucleation and growth are drastically shorted by fast heating of the microwave method. Figure 3 (b) is a schematic illustration of formation process for as-synthesized TiO_2 aggregates by microwave assisted method. The microwave nucleated precursors had higher population of nuclei with smaller sizes than the precursors nucleated by the conventional heating³⁹. During the transient stage of nucleation, so much many small crystals are easy to touch together to be assembled to clusters due to their high surface energy. The rapid heating rate and superheating / "hot spots" of the reaction system under microwave irradiation result in a fast increased reaction rate³⁹. So the clusters grow up rapidly, meanwhile, are assembled to TiO_2 nanocrystallites aggregates.

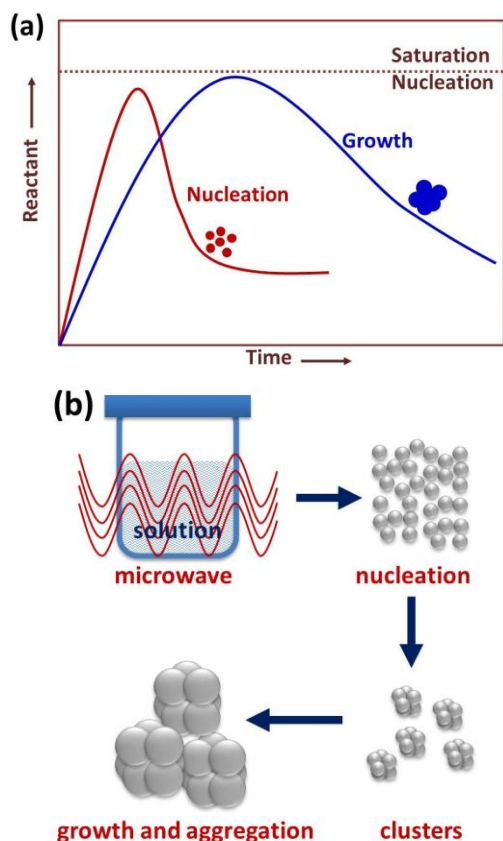


Figure 3. (a) La-Mer model for nucleation and growth kinetics of nanoparticles and (b) schematic illustration of TiO_2 aggregates formation process.

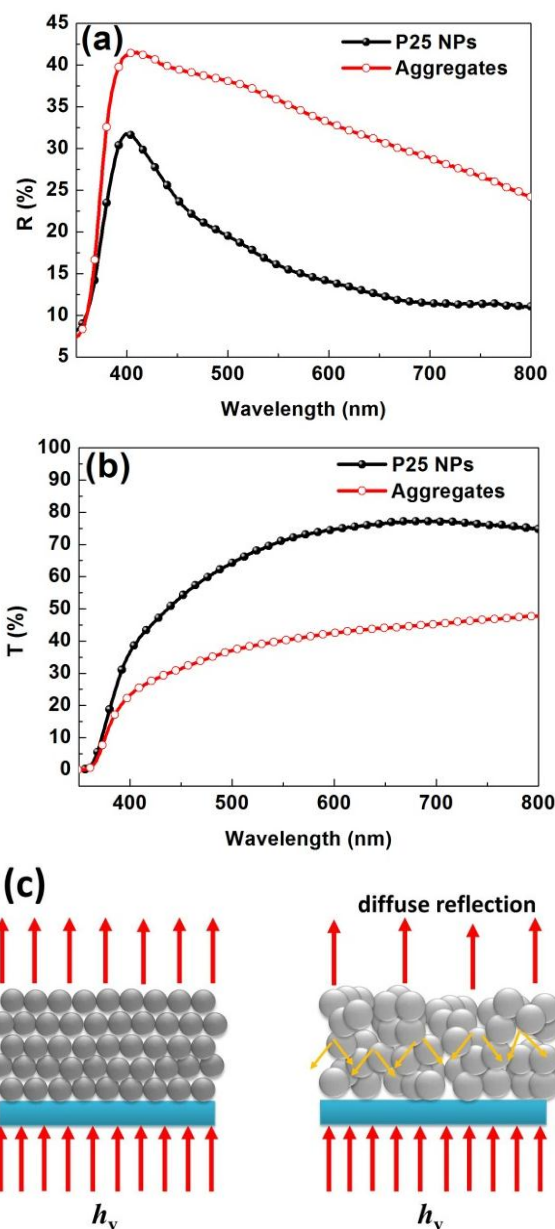


Figure 4. Diffuse reflection (a) and transmittance spectra curves (b) of P25 nanoparticles TiO_2 film and TiO_2 aggregates film, and (c) schematic illustration of the effect of the aggregates for the light scattering.

The light scattering is an important cause for the increase of the absorbance of incident photons for the enhancement of photo-generated current. So the efficient light scattering is necessary for highly performed photoanodes of DSCs¹⁹. Normally, when light encounters an object, according to the laws of reflection and refraction, the radiation may either propagate in the forward direction, giving rise to refraction and absorption, or propagate in the backward direction, causing reflection⁴⁰. So diffuse reflectance and transmittance data can reveal the extent to which incident light is scattered by particles in the photoanodes and how much the incident light passes through the photoanodes without being scattered⁴¹. The ideal light scattering properties of a photoanode should be a high diffuse reflectance and low diffuse transmission. Figure 4 (a) and (b) show the diffuse reflection and transmittance spectra curves of P25 TiO_2 nanoparticles (NPs) and TiO_2 aggregates films without

sensitization. It can be seen that the diffuse reflectance of the TiO₂ aggregates is much stronger than that of TiO₂ NPs in the 400-800 nm range, which is the main wavelength range dye used in DSCs could capture the photons effectively. In addition, the diffuse transmittance of the TiO₂ aggregates film is much weaker than that of TiO₂ NPs film, indicating that there are more photons trapped in the aggregates film. Figure 4 (c) shows a schematic illustration of the effect of the aggregates for the light scattering. The results can be attributed to the strong scattering of the aggregates, which makes the incident light directly reflect back towards the nanoparticles. As a result, incident light could be scattered more efficiently by the ZnO aggregates synthesized by microwave assisted method. Thus the photocurrent and PCE of devices based on TiO₂ aggregates film could be increased by the enhanced light scattering.

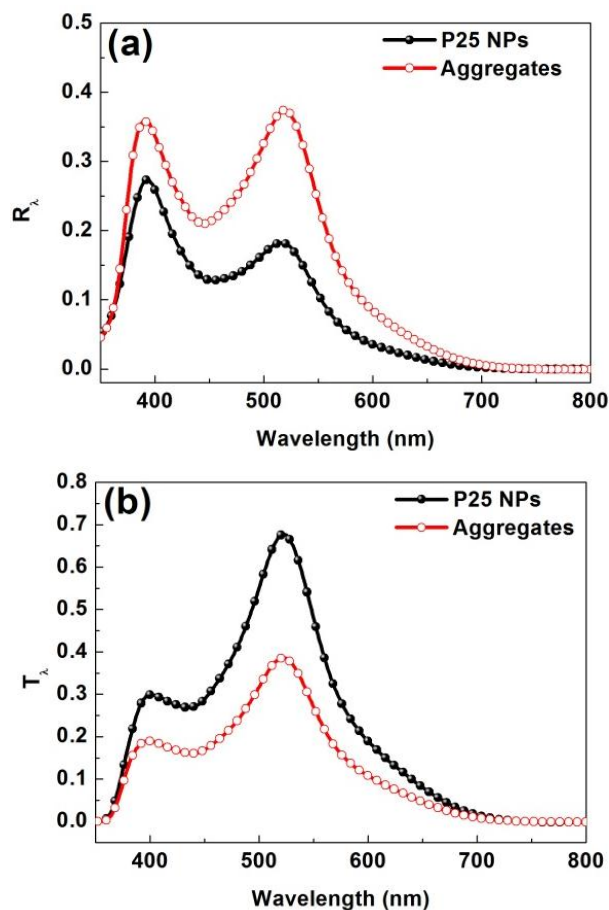


Figure 5. Relative diffuse reflectance (a) and (b) relative diffuse transmittance curves of P25 nanoparticles TiO₂ film and TiO₂ aggregates film.

To further studying the light scattering effects of the different structural TiO₂ films, the ‘‘relative diffuse reflectance (R_r)’’ and ‘‘relative diffuse transmittance (T_r)’’ can be proposed to investigate the light capture of the photoanodes with loading of N719 dye in the range from 350 nm to 800 nm. The R_r and T_r can be calculated from the measured diffuse reflectance and diffuse transmittance using the following equations¹⁹:

$$R_r = \frac{\int_{\lambda_1}^{\lambda_2} I_\lambda R_\lambda d\lambda}{\int_{\lambda_1}^{\lambda_2} I_\lambda d\lambda} \quad (1)$$

$$T_r = \frac{\int_{\lambda_1}^{\lambda_2} I_\lambda T_\lambda d\lambda}{\int_{\lambda_1}^{\lambda_2} I_\lambda d\lambda} \quad (2)$$

where R_λ and T_λ are diffuse reflectance and diffuse transmittance at the certain wavelength, which are measured in Figure 4(a) and (b). I_λ is the normalized absorption spectra intensity of N719 dye at λ wavelength. The λ_1 to λ_2 is corresponding to 350-800 nm in this study. The results are shown in Figure 5(a) and (b), indicating that the TiO₂ aggregates film shows higher R_r and lower T_r than those of TiO₂ NPs film in the 400-700 nm range, which is accorded with the results in Figure 4(a) and (b). Therefore, in the range of spectra which dye could absorb effectively, the TiO₂ aggregates film synthesized by microwave assisted method has better light scattering than P25 nanoparticles film.

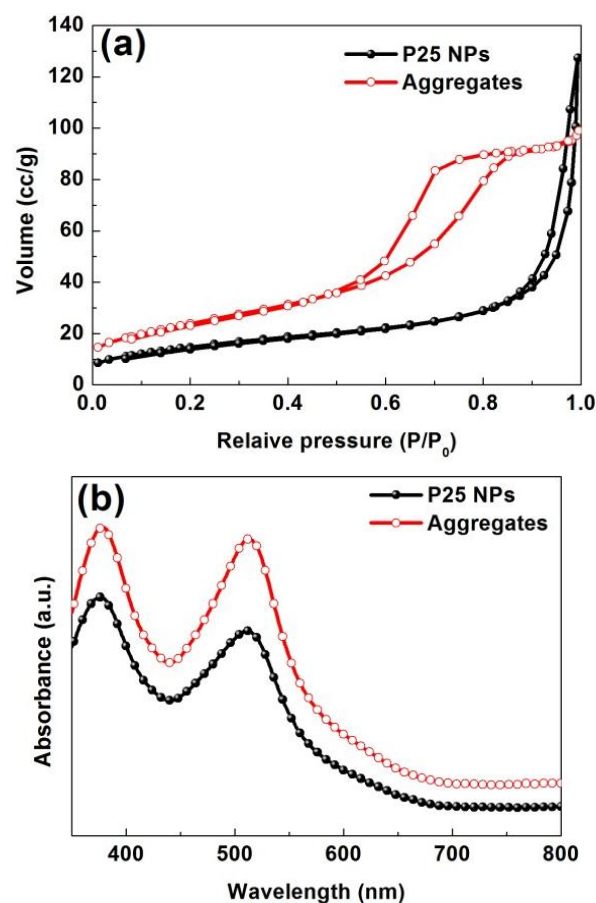


Figure 6. (a) Nitrogen sorption isotherms of P25 and aggregates TiO₂ powders, and (b) UV-vis absorption spectra of the dye (N719) desorbed from the TiO₂ films.

Table 1. Surface properties and dye loading of the different films

Parameters	P25	Aggregates
BET surface area (m ² /g)	53.53	86.90
Pore volume (mL/g)	0.20	0.17
Average pore size (nm)	14.72	7.05
Dye-loading(10 ⁻⁷ mol/cm ²)	1.49	2.42

Figure 6 (a) shows the nitrogen sorption isotherms of P25 and aggregates TiO₂ powders. The detailed surface properties and dye loading are listed in Table 1. It can be seen that the TiO₂

nanocrystallite aggregates has a much higher BET surface area (86.9 m^2/g) than that of the P25 nanoparticles (53.5 m^2/g). However, the pore volume (0.17 mL/g) and average pore size (7.05 nm) are lower than those of P25 nanoparticles (0.20 mL/g and 14.72 nm). The possible cause is that the size of nanocrystallites within the aggregates (~ 10 nm as shown in Figure 2) is smaller than that of P25 nanoparticles (~ 20 nm as shown in the previous work²¹). The average pore size of the aggregates is calculated using the Barret-Joyner-Halender (BJH) method based on the nanocrystallites within the aggregates. But there are a lot of porous channels among the aggregates that facilitate the dye molecules to penetrate into the interior of the mesoporous films. Although the low pore volume is not good for the dye loading, the difference value (0.03 mL/g) between the aggregates and P25 is very small, which has little effect on the dye loading of the films. So the dye adsorption of the films is mainly depended on the specific surface area and surface roughness of the mesoporous films. In order to measure the UV-vis absorption spectra of the dye (N719) absorbed within the films, the dye was desorbed by a 0.5M NaOH solution in water and ethanol (1:1, v/v). The absorption spectra in the visible region of both the P25 and aggregates samples are shown in Figure 6 (b). The calculated amount of dye adsorbed per unit area is 2.42×10^{-7} mol/ cm^2 for the aggregates sample and 1.49×10^{-7} mol/ cm^2 for the P25 nanoparticles sample as shown in Table 1. The aggregates sample displays a higher absorption than the P25 sample, which is good consistent with the result of the specific surface areas. Except specific surface area, the surface roughness of the mesoporous film is also an important factor for the dye loading. The surface roughness factors for the both films can be calculated using the following equation⁴²:

$$SRF = \Gamma_{\text{area}} \times N_A \times A_{\text{dye}} \quad (3)$$

where N_A is Avogadro's number, Γ_{area} is the number of attached dye (mol/ cm^2), and A_{dye} is the surface area of the dye molecule (assumed to be 10^{-14} nm^2). By calculating the SRF value for P25 is 894, while that of the aggregates is 1452. Compared with P25 nanoparticles, the much more dye absorbed within the aggregates film is derived from both the larger specific surface area and higher surface roughness, which is helpful high light photocurrent of the solar cell.

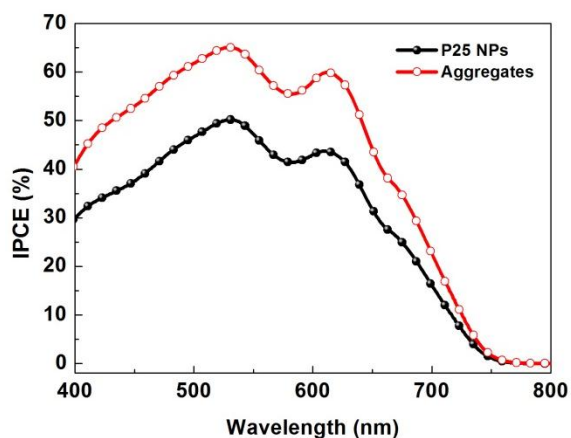


Figure 7. Incident photon-to-current conversion efficiency (IPCE) spectra of the DSCs with different photoanodes.

To further understand the effect of the structure of the photoanodes on the photon-to-current conversion, the incident photon-to-current conversion efficiency (IPCE) spectra have been measured for DSCs with different photoanodes in the range of

wavelengths from 400 to 800 nm as shown in Figure 7. Maximum IPCE of DSC based on aggregates photoanode reaches 65% at 530 nm (the region of maximum light absorption by N719), which is enhanced by $\sim 30\%$ compared to the maximum IPCE of 50% at 530 nm for DSC based on P25 photoanode. IPCE is substantially improved from visible to near infrared radiation region 750 nm. So the improvement of IPCE of DSC assembled by the aggregates is mainly derived from the enhancement of the diffuse reflectance and light absorbance.

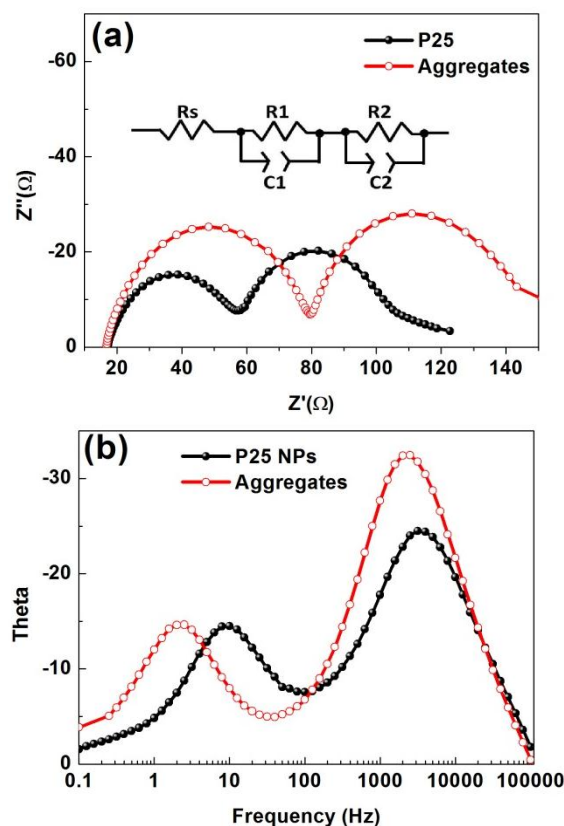


Figure 8. (a) Nyquist plot and (b) Bode plot of DSCs based on the different photoanodes under dark condition.

The measurement of electrochemical impedance spectroscopy (EIS) has been carried out to study the charge transfer property in the DSCs based on the different photoanodes. Figure 8 shows the impedance spectra of the DSCs measured under forward bias (-0.7V) under dark condition. In the Figure 8(a), the two semicircles correspond to the resistances of electron diffusion (R_1), and charge transfer (R_2), respectively at the $\text{TiO}_2/\text{electrolyte}$ interface⁴³. It can be seen that both R_1 and R_2 of DSC based on aggregates are higher those of the one based P25 NPs. The higher R_1 of the aggregates photoanode is attributed to the longer path of electron diffusion in the aggregate structure, which is not beneficial to the photo-current (J_{sc}). However, the R_2 is considered as the charge transfer resistance^{19, 43}. A larger value of R_2 means less surface charge recombination at the sensitized $\text{TiO}_2/\text{electrolyte}$ interface, which facilitates the transfer and collection of electron. In addition, the electron lifetime (τ_n) in the aggregates photoanode is longer than that in P25 photoanode according to Figure 8 (b) ($1/2\pi f_{\text{max}}$)⁴⁴. The main reason is also ascribed to the decrease of surface charge recombination.

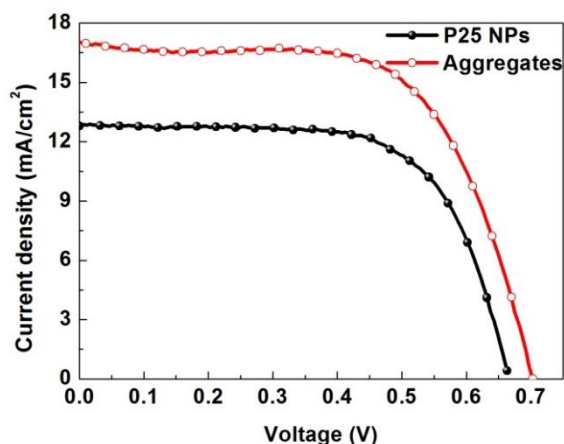


Figure 9. J-V curves of DSCs with different photoanodes.

Table 2. Photovoltaic properties of DSCs with different photoanodes.

Samples	V_{oc} (V)	J_{sc} ($\text{mA}\cdot\text{cm}^{-2}$)	FF	PCE(%)
P25	0.66	12.79	0.66	5.57
Aggregates	0.70	17.05	0.64	7.64

Figure 9 shows the J - V curves for DSCs measured under the illumination of one sun (AM 1.5, $100\text{mW}/\text{cm}^2$). The detailed performance parameters of DSCs based on the different photoanodes are shown in Table 2, where it is obvious that DSCs based on the TiO_2 aggregates prepared by microwave assisted synthesis exhibits high performance: open voltage (V_{oc}) of 0.70 V, short current density (J_{sc}) of 17.05 mA cm^{-2} , fill factor (FF) of 0.64, PCE of 7.64%. Compared to the P25 nanoparticles, J_{sc} of DSC based on the TiO_2 aggregates increased from 12.79 mA cm^{-2} to 17.05 mA cm^{-2} . As discussed above, the larger surface, higher surface roughness and the stronger scattering of the aggregates which leads to the higher dye-loading, more absorbance of the incident photons and higher IPCE those are the primary causes for the enhancement of photocurrent. In addition, the DSC based on aggregates photoanode shows a little better V_{oc} (0.70 V) than that of P25 nanoparticles (0.66 V). The reason is possible attributed to the difference band-gap structure between the aggregates and P25 nanoparticles. As we all known, the maximum value of V_{oc} is determined by the difference between the quasi Fermi level in TiO_2 under illumination and the oxidation potential of the electrolyte⁴⁵. For n-type semiconductor TiO_2 , the quasi Fermi level is close to the conduction band⁴⁶. The commercial P25 nanoparticles are consisted of 71 wt% anatase and 29 wt% rutile nanoparticles, while the aggregate is the pure anatase phase. The band-gap of anatase ($\sim 3.2\text{ eV}$) is a little higher than that of the rutile ($\sim 3.0\text{ eV}$), which results in the increase of V_{oc} of the aggregates in comparison with the P25 nanoparticles. In addition, EIS results have showed that the high recombination resistance of DSC based on the aggregates is beneficial to the enhancement of V_{oc} due to the decrease of the surface charge recombination.

3. Experimental

3.1 Synthesis of TiO_2 aggregates

TiO_2 aggregates were synthesized through the microwave assisted method. First of all, 0.5mL titanium tetrachloride (TiCl_4) was dissolved in 14mL ethanol with continuous stirring to form a homogeneous solution in air. The container with the mixture solution was moved into the microwave reaction device CEM

Discover microwave system. And the reaction parameters were set to: temperature of 150°C , pressure of 300 Pa, power of 200W, time of 10 min. The synthesized precipitate was separated by centrifugation at 6000 rpm for 10 min and rinsed 3 times using ethanol.

3.2 Preparation of the photoanodes

The as-synthesized TiO_2 powder / P25 powder, ethyl cellulose and α -terpineol were compounded with ethyl alcohol in a specific proportion to make the paste as referring to the previous work⁴⁷. The paste was then coated on a fluorine-doped tin oxide (FTO) glass substrate via the doctor blading method. The as received TiO_2 films underwent a sintering process in air as follows: 125°C for 30 min and at 500°C for 30 min at heating speed of $5^\circ\text{C}/\text{min}$. to get mesoporous films. The thickness of the films sintered is $15\text{--}20\ \mu\text{m}$. The TiO_2 films were immersed in 0.5 mM N719 ethyl solution for 24h at room temperature under dark light.

3.3 Characterization

The scanning electron microscopy (SEM, JSM-7000) and transmission electron microscopy (TEM, Tecnai G2 F20) were used with the purpose of characterize the morphology of the TiO_2 aggregates. And the crystal structures of the TiO_2 aggregates were tested by X-ray diffraction (XRD) on an X'Pert PROS (Philips Co.) with a radiation of Cu-K α ($\lambda = 0.154060\ \text{\AA}$). N_2 adsorption-desorption isotherms were recorded on ASAP2020 instrument (Micromeritics Co.), and the specific surface areas (S_{BET}) were calculated using the BET equation. Desorption isotherm was used to determine the pore size distribution using the Barret-Joyner-Halender (BJH) method. The concentration of desorbed dye in film was calculated from UV-vis absorption spectra (UV-3600, Shi-madzu). The electrochemical impedance spectroscopy (EIS) measurements were also performed with the electrochemical workstation (Zahner, Zennium). The photovoltaic performance of DSCs was measured under a solar simulator (Oriol Sol 3A Solar Simulator, 94063A, Newport Stratford Inc.), equipped with a 300 W xenon lamp (Newport) and a Keithley digital source meter (Keithley, 2400) controlled by Testpoint software. The properties of the solar cells were tested under AM 1.5 simulated sunlight with an output power density of $100\text{ mW}/\text{cm}^2$.

Conclusions

The nearly spherical TiO_2 aggregates with size of $\sim 500\text{ nm}$ consisted of $\sim 10\text{ nm}$ nanocrystallites have been prepared by microwave assisted method at 150°C for 10 minutes. The rapid heating rate and superheating / "hot spots" of the reaction system under microwave irradiation result in a huge amounts of nucleuses in a short time so as to form a great deal of clusters. The clusters grow up rapidly, meanwhile, are assembled to TiO_2 nanocrystallite aggregates. The TiO_2 aggregates show the better light scattering property, larger specific surface area and higher dye-loading than those of the commercial P25 TiO_2 nanoparticles. In comparison with P25, the short current density (J_{sc}) and dye-loading of DSC based the as-synthesized TiO_2 aggregates increase by 33% and 62%, respectively. At a result, the PCE of the DSC is up to 7.64%.

Acknowledgements

This work was supported by the National Science Foundation of China (51374029), Program for New Century Excellent Talents in University (NCET-13-0668) and Fundamental Research Funds for the Central Universities (FRF-TP-14-008C1). This work was also supported by the "thousands talents" program for pioneer researcher and his innovation team, China.

Notes and references

- ^a Advanced Materials and Technology Institute, University of Science and Technology Beijing, 100083, China.
- ^b Beijing Institute of Nanoenergy and Nanosystems, Chinese Academy of Sciences, 100083, China
- ^c Department of Materials and Engineering, University of Washington, Seattle, WA 98195-2120, USA.
- *Corresponding authors:**
tianjianjun@mater.ustb.edu.cn
- E. J. W. Crossland, N. Noel, V. Sivaram, T. Leijtens, J. A. Alexander-Webber and H. J. Snaith, *Nature*, 2013, **495**, 215-219.
 - J. S. Chen, Y. L. Tan, C. M. Li, Y. L. Cheah, D. Y. Luan, S. Madhavi, F. Y. C. Boey, L. A. Archer and X. W. Lou, *J. Am. Chem. Soc.*, 2010, **132**, 6124-6130.
 - B. Oregan and M. Gratzel, *Nature*, 1991, **353**, 737-740.
 - C. J. Barbe, F. Arendse, P. Comte, M. Jirousek, F. Lenzmann, V. Shklover and M. Gratzel, *J. Am. Ceram. Soc.*, 1997, **80**, 3157-3171.
 - M. K. Nazeeruddin, P. Pechy, T. Renouard, S. M. Zakeeruddin, R. Humphry-Baker, P. Comte, P. Liska, L. Cevey, E. Costa, V. Shklover, L. Spiccia, G. B. Deacon, C. A. Bignozzi and M. Gratzel, *J. Am. Chem. Soc.*, 2001, **123**, 1613-1624.
 - R. Gao, L. Wang, Y. Geng, B. Ma, Y. Zhu, H. Dong and Y. Qiu, *Journal of Physical Chemistry C*, 2011, **115**, 17986-17992.
 - R. Gao, L. Wang, B. Ma, C. Zhan and Y. Qiu, *Langmuir*, 2010, **26**, 2460-2465.
 - T. Kinoshita, J. T. Dy, S. Uchida, T. Kubo and H. Segawa, *Nat. Photonics*, 2013, **7**, 535-539.
 - K. Lee, S. W. Park, M. J. Ko, K. Kim and N. G. Park, *Nat. Mater.*, 2009, **8**, 665-671.
 - J.-Y. Liao, J.-W. He, H. Xu, D.-B. Kuang and C.-Y. Su, *J. Mater. Chem.*, 2012, **22**, 7910-7918.
 - S. Mathew, A. Yella, P. Gao, R. Humphry-Baker, B. F. E. Curchod, N. Ashari-Astani, I. Tavernelli, U. Rothlisberger, M. K. Nazeeruddin and M. Graetzel, *Nat. Chem.*, 2014, **6**, 242-247.
 - X. Feng, K. Zhu, A. J. Frank, C. A. Grimes and T. E. Mallouk, *Angew. Chem.*, 2012, **51**, 2727-2730.
 - Y. J. Kim, M. H. Lee, H. J. Kim, G. Lim, Y. S. Choi, N.-G. Park, K. Kim and W. I. Lee, *Adv. Mater.*, 2009, **21**, 3668-3673.
 - J. Wang and Z. Lin, *Chem. Mater.*, 2008, **20**, 1257-1261.
 - M. D. Ye, X. K. Xin, C. J. Lin and Z. Q. Lin, *Nano Lett.*, 2011, **11**, 3214-3220.
 - J. Lin, Y. U. Heo, A. Nattestad, Z. Sun, L. Wang, J. H. Kim and S. X. Dou, *Sci. Rep.*, 2014, **4**, 5769.
 - R. Gao, J. Tian, Z. Liang, Q. Zhang, L. Wang and G. Cao, *Nanoscale*, 2013, **5**, 1894-1901.
 - W. Wang, H. Zhang, R. Wang, M. Feng and Y. Chen, *Nanoscale*, 2014.
 - R. Gao, Z. Liang, J. Tian, Q. Zhang, L. Wang and G. Cao, *Nano Energy*, 2013, **2**, 40-48.
 - T. P. Chou, Q. F. Zhang, G. E. Fryxell and G. Z. Cao, *Adv. Mater.*, 2007, **19**, 2588-2592.
 - J. Xi, Q. Zhang, K. Park, Y. Sun and G. Cao, *Electrochim. Acta*, 2011, **56**, 1960-1966.
 - Q. F. Zhang, T. R. Chou, B. Russo, S. A. Jenekhe and G. Z. Cao, *Angew. Chem.Int. Edit.*, 2008, **47**, 2402-2406.
 - Q. Zhang, E. Uchaker, S. L. Candelaria and G. Cao, *Chem. Soc. Rev.*, 2013, **42**, 3127-3171.
 - Q. F. Zhang and G. Z. Cao, *Nano Today*, 2011, **6**, 91-109.
 - Q. F. Zhang and G. Z. Cao, *J. Mater. Chem.*, 2011, **21**, 6769-6774.
 - M. J. Alam and D. C. Cameron, *J. Sol-Gel Sci. Techn.*, 2002, **25**, 137-145.
 - K.-i. Katsumata, Y. Ohno, K. Tomita, T. Taniguchi, N. Matsushita and K. Okada, *Acs Appl. Mater. Interfaces*, 2012, **4**, 4846-4852.
 - C.-T. Dinh, T.-D. Nguyen, F. Kleitz and T.-O. Do, *Acs Nano*, 2009, **3**, 3737-3743.
 - T. R. Gordon, M. Cargnello, T. Paik, F. Mangolini, R. T. Weber, P. Fornasiero and C. B. Murray, *J. Am. Chem. Soc.*, 2012, **134**, 6751-6761.
 - I. Bilecka and M. Niederberger, *Nanoscale*, 2010, **2**, 1358-1374.
 - M. I. Dar, A. K. Chandiran, M. Gratzel, M. K. Nazeeruddin and S. A. Shivashankar, *J. Mater. Chem. A*, 2014, **2**, 1662-1667.
 - K. Manseki, Y. Kondo, T. Ban, T. Sugiura and T. Yoshida, *Dalton Trans.*, 2013, **42**, 3295-3299.
 - K. F. Moura, J. Maul, A. R. Albuquerque, G. P. Casali, E. Longo, D. Keyson, A. G. Souza, J. R. Sambrano and I. M. G. Santos, *J. Solid State Chem.*, 2014, **210**, 171-177.
 - Asdim, K. Manseki, T. Sugiura and T. Yoshida, *New J. Chem.*, 2014, **38**, 598-603.
 - P.-S. Shen, Y.-C. Tai, P. Chen and Y.-C. Wu, *J. Power Sources*, 2014, **247**, 444-451.
 - M. Cargnello, T. R. Gordon and C. B. Murray, *Chem. rev.*, 2014.
 - A. R. Tao, S. Habas and P. D. Yang, *Small*, 2008, **4**, 310-325.
 - G. Cao and Y. Wang, *Nanostructures and Nanomaterials*, World Scientific Publishing Co. Pte. Ltd., Singapore, 2011.
 - Y. J. Zhu and F. Chen, *Chem. rev.*, 2014, **114**, 6462-6555.
 - Q. Zhang, D. Myers, J. Lan, S. A. Jenekhe and G. Cao, *Phys. Chem. Chem. Phys.*, 2012, **14**, 14982-14998.
 - J. Tian, L. Lv, X. Wang, C. Fei, X. Liu, Z. Zhao, Y. Wang and G. Cao, *J. Phys. Chem. C*, 2014, **118**, 16611-16617.
 - N. A. Dahoudi, J. Xi and G. Cao, *Electrochim. Acta*, 2012, **59**, 32-38.
 - Y. Shi, K. Wang, Y. Du, H. Zhang, J. Gu, C. Zhu, L. Wang, W. Guo, A. Hagfeldt, N. Wang and T. Ma, *Adv. Mater.*, 2013, **25**, 4413-4419.
 - J. Bisquert, F. Fabregat-Santiago, I. Mora-Sero, G. Garcia-Belmonte and S. Gimenez, *J. Phys. Chem. C*, 2009, **113**, 17278-17290.
 - P. Chen, J. H. Yum, F. De Angelis, E. Mosconi, S. Fantacci, S.-J. Moon, R. H. Baker, J. Ko, M. K. Nazeeruddin and M. Graetzel, *Nano Lett.*, 2009, **9**, 2487-2492.
 - B. Liu, X. Wang, L. Wen and X. Zhao, *Chem-Eur. J.*, 2013, **19**, 10751-10759.
 - J. J. Tian, R. Gao, Q. F. Zhang, S. G. Zhang, Y. W. Li, J. L. Lan, X. H. Qu and G. Z. Cao, *J. Phys. Chem. C*, 2012, **116**, 18655-18662.